BeBeC-2026-S07

OPTIMAL ARRAY MICROPHONE ARRANGEMENTS REVISITED

Ennes Sarradj and Adam Kujawski
TU Berlin, FG Technische Akustik
Einsteinufer 25, 10587 Berlin, Germany

Abstract

The spatial arrangement of microphones strongly influences the performance of acoustic imaging methods. Previous studies have shown that phyllotaxis-based sunflower arrays provide favorable beamforming characteristics for disk-like apertures. However, practical applications often require non-circular geometries and more flexible array-generation strategies.

The present work investigates planar microphone arrangements based on weighted Vogel spirals and compares several methods for adapting such arrangements to non-circular domains. Beamforming performance is evaluated using point spread function characteristics, including main-lobe width, maximum side-lobe level, and integrated side-lobe level. The results confirm the Pareto-like trade-off between spatial resolution and side-lobe suppression previously reported for weighted sunflower arrays. In addition, geometric mapping, masking, and weighted centroidal Voronoi tessellation are investigated for square, rectangular, and cross-shaped apertures.

The results show that all investigated adaptation methods provide comparable performance for mildly non-circular geometries, while weighted centroidal Voronoi tessellation yields the most robust overall behavior for more complex domains. The study demonstrates that favorable spatial sampling properties can be preserved beyond circular apertures, provided that the resulting arrangements maintain a sufficiently homogeneous and isotropic distribution of pairwise microphone separations.

1 Introduction

Microphone arrays are widely used for acoustic source localization and sound-field reconstruction in applications ranging from aeroacoustic wind-tunnel measurements to machine diagnostics and room acoustics. The spatial arrangement of the microphones strongly influences the

quality of the resulting acoustic images, since the array geometry determines the spatial sampling properties and therefore the point spread function (PSF) of the reconstruction method. In particular, the achievable spatial resolution, side-lobe behavior, and robustness against imaging artifacts depend critically on the distribution of pairwise microphone separations within the array.

Early microphone-array designs were often based on regular grids or concentric ring structures because of their simple construction and straightforward analysis. However, such arrangements tend to produce strong grating lobes and highly redundant coarray structures, especially at higher frequencies. To mitigate these effects, a large variety of irregular and deterministic aperiodic geometries have been proposed. Classical deterministic aperiodic arrangements include logarithmic spiral arrays, such as the Dougherty spiral [1], and multi-arm equal-area spiral variants commonly associated with Underbrink [2].

Over the past decade, phyllotaxis-based or sunflower-type arrangements have received particular attention. Inspired by naturally occurring phyllotactic patterns, Vogel spirals combine irrational angular increments with area-based radial distributions and thereby provide highly homogeneous spatial sampling properties. Sarradj [3] introduced a generalized synthesis framework for such arrays and demonstrated that weighted phyllotactic arrangements form approximately Pareto-optimal trade-offs between beam width and side-lobe suppression. Subsequent studies confirmed the favorable beamforming and holography performance of sunflower arrays for practical acoustic imaging applications [4].

Besides deterministic constructions, a substantial body of work has investigated numerical optimization approaches for microphone-array synthesis. Techniques based on genetic algorithms, particle swarm optimization, differential evolution, Bayesian optimization, and topology optimization have been proposed to optimize microphone positions with respect to beamforming quality metrics [5–10]. While these methods can produce highly specialized array geometries, the resulting layouts often depend strongly on the chosen objective function and optimization strategy, and global optimality is generally difficult to establish in the high-dimensional non-convex design space.

Most previous studies have focused on disk-like planar arrays because such geometries naturally arise from spiral-based synthesis methods and provide favorable isotropic aperture coverage. In practical applications, however, the available installation space is often non-circular. Wind-tunnel arrays, vehicle-mounted arrays, and measurement-window configurations frequently require rectangular, elongated, cross-shaped, or otherwise constrained geometries, sometimes including holes or excluded regions. Comparatively little attention has been devoted to the question of how the favorable spatial sampling properties of phyllotactic arrangements can be preserved under such geometric constraints.

The present work therefore investigates several strategies for adapting weighted Vogel-type microphone arrangements to non-circular planar domains. In addition to geometric mappings and masking procedures, weighted centroidal Voronoi tessellation (CVT) is considered as a flexible synthesis approach for arbitrary aperture shapes. The resulting arrangements are evaluated using beamforming-based PSF characteristics, including main-lobe width, maximum side-lobe level, and integrated side-lobe level. The study compares classical spiral geometries with generalized phyllotactic arrangements and analyzes the extent to which favorable beamforming properties can be retained for non-circular apertures.

The remainder of this paper is structured as follows. Section 2 introduces the theoretical

background and reviews relevant array synthesis strategies. Section 3 describes the investigated geometry adaptation methods. Section 4 presents the evaluation methodology and performance metrics. Section 5 discusses the beamforming results for circular and non-circular geometries, and Section 6 summarizes the conclusions and perspectives for future work.

2 Background and Theoretical Considerations

The suitability of a microphone arrangement for acoustic imaging can be assessed by its response to an elementary source. For linear imaging methods, the response to a point source is described by the point spread function (PSF), which characterizes how an ideal point source is represented in the reconstructed source map. The PSF therefore provides a direct link between the microphone coordinates and practically relevant imaging properties such as resolution, side-lobe level, and dynamic range. For conventional beamforming, the PSF is directly determined by the steering vectors associated with the microphone positions and the scanning grid. It therefore provides a natural first criterion for evaluating microphone arrangements. Other methods, such as deconvolution and inverse methods, are designed to mitigate the effects of the PSF, but it can be assumed their performance will still be influenced by the underlying PSF characteristics. Therefore, the PSF can be considered a fundamental property of the array geometry that influences the performance of various signal processing techniques.

2.1 PSF properties and array design requirements

Several properties of the PSF are relevant for array design. The width of the main lobe determines the spatial resolution of the reconstructed source map, while the level and distribution of side lobes determine the extent to which false source locations or ghost sources may appear. An array geometry is therefore desirable if it produces a compact main lobe, low and diffuse side lobes, and limited orientation-dependent artifacts over the frequency range of interest.

These PSF characteristics can be related to the spatial sampling properties of the array. In particular, the distribution of pairwise microphone separations, commonly referred to as the coarray, determines which spatial phase differences are sampled. In general, favorable PSF characteristics are associated with a coarray that covers the relevant range of spatial frequencies broadly and approximately uniformly, while avoiding excessive clustering, large unsampled regions, and strong directional bias. The density and distribution of these points in the coarray plane directly influence the shape of the PSF. For example, a broad and approximately uniform distribution of coarray points supports high spatial resolution and tends to reduce coherent side-lobe structures, while clustering of coarray points can lead to increased side lobes and orientation-dependent artifacts.

These considerations suggest several design requirements for planar microphone arrays. First, the microphones should be arranged in a way that promotes a broad and approximately uniform distribution of pairwise separations. Second, the arrangement should avoid regular patterns, which may give rise to clustered coarray points and strong side lobes. Third, the array should cover the spatial frequencies of interest for the application, which requires an appropriate combination of aperture size and microphone density. A fourth, additional requirement is that the array should remain compact and fit within a prescribed physical area, which is often a practical constraint in real-world applications.

2.2 Some array synthesis strategies

The requirements outlined above define an idealized array design problem. The microphone positions should lead to favorable PSF characteristics and a well-conditioned spatial sampling behavior, while simultaneously satisfying constraints on aperture size, number of microphones, and array boundary. Since these requirements are partly competing, optimality cannot generally be understood with respect to a single scalar criterion. Instead, array performance is more appropriately considered in a multi-objective sense, where an arrangement is optimal if no relevant performance criterion can be improved without degrading at least one other criterion.

Several strategies have been proposed to construct such arrangements. A direct approach is numerical optimization, in which the microphone coordinates are iteratively refined according to one or more prescribed objective functions. Although this strategy can produce high-performing layouts for a given formulation, the resulting arrangements depend strongly on the chosen objective function, constraints, initialization, and optimization algorithm. Moreover, because the design space is high-dimensional and generally non-convex, numerical optimization does not by itself demonstrate global optimality, and different runs may lead to different local solutions.

An alternative approach is to use deterministic aperiodic geometries that possess favorable spatial sampling properties by construction. Spiral arrangements are particularly attractive in this respect, since they combine compact aperture coverage, rotational uniformity, absence of translational periodicity, and controllable radial density. In particular, phyllotaxis-based or sunflower-like arrays have been shown to provide favorable compromises between competing array-performance criteria and can therefore be interpreted as Pareto-optimal candidates within appropriately defined design spaces. For this reason, spiral-based synthesis methods provide a useful starting point for the construction and adaptation of microphone arrangements considered in this work.

Thus, the role of an array synthesis method is not to produce a universally optimal geometry, but to generate candidate layouts that achieve a favorable trade-off between the relevant array-response properties under the given physical constraints. Well-known examples of deterministic aperiodic synthesis methods are spiral-based arrangements, in which the microphones are positioned according to analytically defined curves or point distributions. Without further modifications, such arrangements typically produce disk-like geometries. Some of these are proposed by and named after Dougherty and Underbrink, respectively. A third example is the so-called Vogel spiral, which is based on the golden angle and is commonly observed in natural phyllotactic patterns.

The Dougherty spiral is based on a logarithmic spiral with microphones placed at equal arc-length intervals along the curve. The design is specified by the minimum and maximum radii r_0 and $r_{\max}$, the number of microphones N, and the spiral angle ν, which defines the constant angle at which the spiral intersects radial lines. With the arc-length coordinate

$$l_n = \frac{n-1}{N-1} l_{\max}, \qquad n = 1, \ldots, N, \tag{1}$$

and

$$l_{\max} = \frac{r_0 \sqrt{1+\cot^2(\nu)}}{\cot(\nu)} \left(\frac{r_{\max}}{r_0} - 1 \right), \tag{2}$$

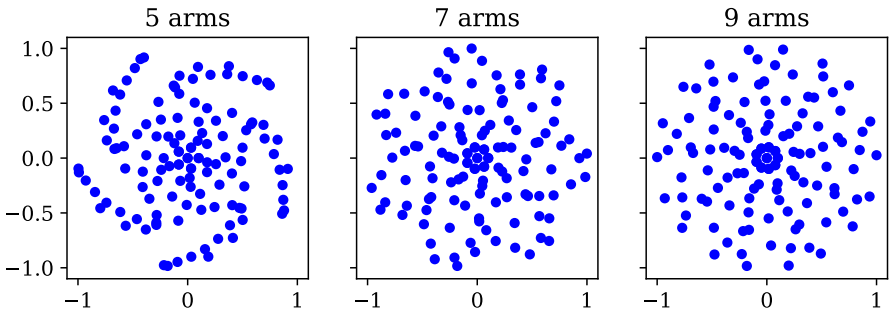

Figure 1: Example geometries of the Dougherty spiral for different number of arms and $\nu = \frac{15\pi}{32}$, $r_0 = 0.1$, $r_{\max} = 1.0$ *and* $N = 64$

the microphone positions are obtained from

$$\theta_n = \frac{1}{\cot(\nu)} \ln\left(1 + \frac{\cot(\nu) l_n}{r_0 \sqrt{1+\cot^2(\nu)}}\right), \qquad r_n = r_0 \exp(\cot(\nu)\theta_n). \tag{3}$$

This construction yields a deterministic aperiodic layout with increasing radius and non-uniform angular spacing. It is attractive for beamforming because the logarithmic spiral avoids the translational periodicity of regular grids and tends to produce a non-redundant distribution of microphone separations. The single-arm nature of the array, however, may lead to an uneven distribution of microphones and an extension to multi-arm spiral variants is desirable (Fig. 1).

The Underbrink spiral can be interpreted as a modified multi-arm logarithmic spiral. Instead of placing microphones at equal arc-length intervals, the aperture is divided into equal-area annular segments, and microphones are positioned near the centers of these segments. For N_a spiral arms and N_m microphones per arm, the radial coordinates are commonly written as

$$r_{m,1} = r_0, \qquad m = 1, \ldots, N_a, \tag{4}$$

and

$$r_{m,n} = r_{\max} \sqrt{\frac{2n-3}{2N_m - 3}}, \qquad m = 1, \ldots, N_a, \quad n = 2, \ldots, N_m. \tag{5}$$

The angular coordinates follow the logarithmic spiral relation with an additional rotation for each arm,

$$\theta_{m,n} = \frac{\ln(r_{m,n}/r_0)}{\cot(\nu)} + \frac{m-1}{N_a} 2\pi, \qquad m = 1, \ldots, N_a, \quad n = 1, \ldots, N_m. \tag{6}$$

This arrangement combines the aperiodicity of logarithmic spirals with a more balanced aperture coverage than a single-arm design. The equal-area radial construction distributes microphones more evenly over the disk, while the multiple rotated arms (Fig. 2) improve angular coverage and typically yield favorable beamwidth and sidelobe behavior in comparison studies.

The Vogel spiral [11], often also referred to as the sunflower or phyllotaxis spiral, is a deterministic aperiodic point distribution inspired by the arrangement of seeds in sunflower heads.

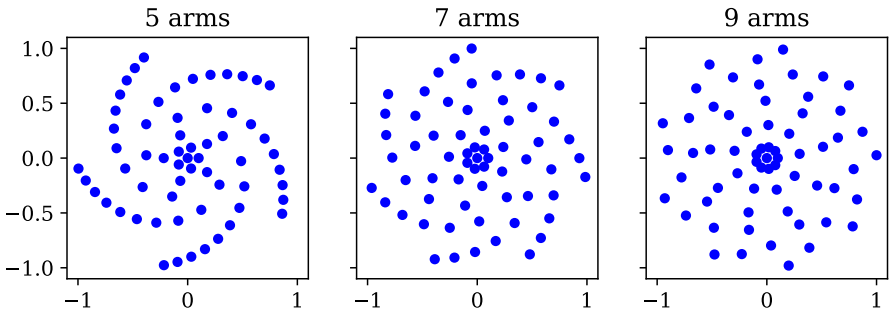

Figure 2: Example geometries of the Underbrink spiral for different number of arms and $\nu = \frac{5\pi}{8}$, $r_0 = 0.1$, $r_{\max} = 1.0$ *and* $N = 64$

In contrast to logarithmic spiral arrays such as the Dougherty and Underbrink spirals, the Vogel spiral places successive points according to a constant angular increment and a radially increasing distance from the center. For a planar array with N microphones and maximum radius $r_{\max}$, the microphone positions are commonly defined by

$$r_n = r_{\max}\sqrt{\frac{n}{N}}, \qquad n = 1,\ldots,N, \tag{7}$$

and

$$\theta_n = n\pi(1+\sqrt{V}), \tag{8}$$

where $V = 5$ yields the classical sunflower pattern corresponding to the golden-angle increment.

The square-root dependence of the radius on the index n is chosen so that the points are approximately uniformly distributed with respect to area rather than radius. Since the area of a disk grows proportionally to r^2, this radial law prevents excessive clustering near the outer boundary and produces an approximately constant average point density over the aperture. The irrational angular increment avoids the formation of repeated angular alignments and prevents the microphones from falling onto a limited number of radial spokes, as would occur for rational angular increments. This combination of area-based radial placement and irrational angular rotation leads to a compact, rotationally balanced, and non-periodic distribution of microphones.

For microphone array design, the Vogel spiral is attractive because it provides a simple closed-form construction with favorable spatial sampling properties. It avoids the strong periodicity of regular grids while maintaining a disk-like aperture and a relatively homogeneous distribution of sensors. Consequently, the resulting coarray tends to be less dominated by repeated separation vectors than that of regular arrangements, which is beneficial for suppressing coherent sidelobe structures in beamforming. At the same time, the deterministic nature of the construction makes the array reproducible and easy to parameterize. The Vogel spiral therefore provides a useful starting point for microphone-array synthesis. Previous work has generalized sunflower-type microphone arrays by introducing tunable radial weighting and has shown that suitable parameter choices can yield Pareto-optimal beamforming properties [3].

2.3 Radial Weighting Strategy

In addition to the geometric arrangement of microphones, the effective aperture weighting strongly influences the resulting point spread function. In classical continuous-aperture theory, spatial weighting functions are commonly used to shape the aperture response in order to control the trade-off between main-lobe width and side-lobe suppression. Depending on the chosen weighting, the resulting PSF may exhibit narrower main lobes, reduced side-lobe levels, or improved robustness against directional artifacts.

Many such weighting functions were originally developed for continuously sampled apertures, where the aperture amplitude varies smoothly as a function of position. Well-known examples include Gaussian, Dolph–Chebyshev, and Hansen-type weightings [12]. In the context of sparse microphone arrays, however, directly applying amplitude weights to the microphone signals may reduce the effective contribution of individual sensors and can decrease the usable dynamic range of the array.

An alternative approach is to realize the desired aperture weighting geometrically rather than electronically. Instead of modifying the signal amplitudes after acquisition, the spatial density of microphones is adjusted such that regions associated with larger aperture weights contain a higher concentration of sensors. In this interpretation, the microphone distribution itself approximates the desired continuous aperture weighting.

In the present work, the weighting strategy proposed by [3] is adopted, which is based on the Hansen weighting function. The corresponding radial weighting modifies the density of microphones as a function of distance from the array center while preserving the deterministic aperiodic structure of the underlying phyllotaxis arrangement. This approach allows the spatial sampling properties of the array to be adapted continuously without introducing the strong periodicity associated with regular grids.

The resulting weighted phyllotaxis arrangements serve as the basis for the subsequent geometry transformations and domain-adaptation procedures considered in this study.

Following the approach proposed by Sarradj, the radial microphone density is controlled by a Hansen-type weighting function. Instead of applying amplitude weights to the microphone signals, the weighting is realized geometrically through a modified radial distribution of the array elements. The corresponding weighting function is defined as

$$f_H(r) = I_0\left(\pi H\sqrt{1-\left(\frac{r}{R}\right)^2}\right)^{\operatorname{sgn}(H)}, \tag{9}$$

where r denotes the radial coordinate, R is the maximum array radius, I_0 is the modified Bessel function of the first kind, and H is a parameter controlling the radial weighting strength. The special case $H = 0$ corresponds to the unweighted Vogel spiral, while positive values of H modify the microphone density toward the center and negative H toward outer regions of the aperture. In this way, the spatial distribution of microphones approximates a continuously weighted aperture while preserving the deterministic aperiodic structure of the phyllotaxis arrangement.

The radial weighting is realized by replacing the uniformly spaced radial coordinate of the Vogel spiral with a sequence of weighted radii. The normalized radius $\rho \in [0,1]$ is divided into M intervals such that each interval contains the same amount of prescribed radial weight. This is done by introducing the antiderivative of the weighting function, a cumulative weighting

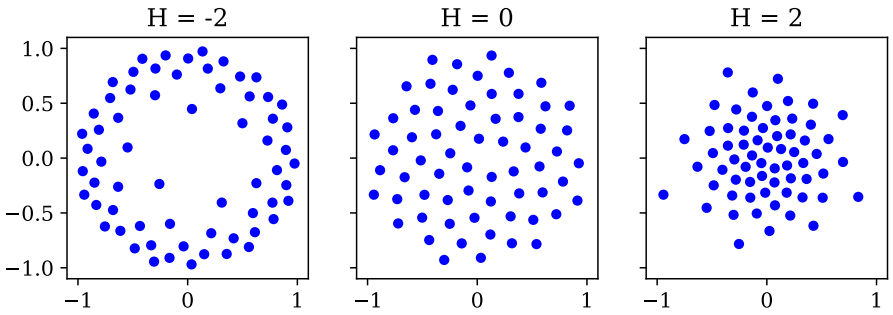

Figure 3: Example geometries of the weighted Vogel spiral for different weighting parameters H and $N = 64$

function $F_H(\rho)$, and determining the radii ρ_i from

$$F_H(\rho_i) - F_H(\rho_{i-1}) = \frac{q}{M}, \qquad i = 1, \ldots, M, \tag{10}$$

with

$$q = F_H(1) - F_H(0), \qquad \rho_0 = 0. \tag{11}$$

For non-negative values of the weighting parameter H, the implementation uses the closed-form expression

$$F_H(\rho) = \frac{1}{2}\left(\rho^2 - 1\right) {}_0F_1\left(2; -\frac{1}{4}H^2\pi^2\left(\rho^2 - 1\right)\right), \tag{12}$$

where ${}_0F_1$ denotes the confluent hypergeometric limit function. The radii ρ_i are obtained successively by solving the nonlinear equation

$$F_H(\rho_i) - F_H(\rho_{i-1}) - \frac{q}{M} = 0 \tag{13}$$

with a scalar root-finding method. Finally, the resulting normalized radii are rescaled to the desired physical aperture radius according to

$$r_i = r_{\max}\frac{\rho_i}{\max_j \rho_j}. \tag{14}$$

In this way, the radial microphone positions are redistributed so that equal increments in microphone index correspond to equal increments of the chosen cumulative radial weighting, rather than to equal increments in radius or area (Fig. 3).

2.4 Geometric adaptation strategies

The weighting strategy described above modifies the radial density of a disk-like phyllotactic arrangement while preserving its circular aperture. However, practical microphone arrays are not always constrained to circular geometries. Mounting frames, wind-tunnel walls, vehicle surfaces, or measurement windows may require rectangular, elongated, or otherwise non-circular apertures. In such cases, the favorable sampling properties of spiral-based arrangements have

to be transferred to a different domain without reintroducing regularity or excessive clustering. This motivates the use of geometric adaptation strategies, some of which are proposed in the following.

A possible strategy for adapting disk-like arrangements to polygonal domains is to use a mapping from the unit disk to the target polygon. In principle, conformal mappings from the unit disk to polygonal domains can be constructed using Schwarz–Christoffel transformations [13]. However, this requires the solution of a parameter problem and may be unnecessarily involved for the present purpose. A simpler approximate alternative is to divide the circular aperture into angular sectors and map each sector to a triangle formed by the polygon center and one polygon edge. Let $\mathbf{c}$ denote the polygon center and let $\mathbf{p}_k$ and $\mathbf{p}_{k+1}$ be two neighboring polygon vertices. A point in the corresponding disk sector is described by its normalized radius $\rho \in [0,1]$ and angular interpolation parameter

$$t = \frac{\theta - \alpha_k}{\alpha_{k+1} - \alpha_k}, \qquad 0 \leq t \leq 1, \tag{15}$$

where α_k and α_{k+1} define the angular bounds of the sector. The point is then mapped to the polygon by

$$\mathbf{x}(\rho, t) = (1-\rho)\mathbf{c} + \rho\left[(1-t)\mathbf{p}_k + t\mathbf{p}_{k+1}\right]. \tag{16}$$

This construction maps the center of the disk to the polygon center and the outer circular boundary of each sector to the corresponding polygon edge. Although the mapping is not conformal and does not preserve distances or local angles exactly, it provides a simple deterministic way to transfer a circular microphone arrangement to a polygonal aperture while preserving the radial ordering and avoiding the introduction of regular grid structures.

The resulting arrangement depends on the choice of the center point $\mathbf{c}$. This point determines the subdivision of the polygon into triangles and therefore controls how the circular sectors are stretched or compressed during the mapping. If $\mathbf{c}$ is chosen poorly, some triangles may become very narrow or strongly distorted, which can lead to local clustering, large empty regions, or an unintended directional bias in the transformed array. The center should therefore be selected carefully, for example as a geometric centroid, an area centroid, or another application-specific reference point that yields a balanced triangulation of the polygonal aperture.

Another simple strategy is to generate a circular phyllotactic arrangement that fully covers the desired polygonal aperture and subsequently remove all microphones outside the target domain. If Ω denotes the polygonal array region and $\mathbf{x}_n$ are the microphone positions of an initially larger circular arrangement, the masked array is given by

$$\mathscr{A}_\Omega = \{\mathbf{x}_n \in \mathscr{A}_{\text{circ}} \mid \mathbf{x}_n \in \Omega\}. \tag{17}$$

This approach preserves the local structure of the original spiral distribution inside the retained region and is straightforward to implement for arbitrary polygonal boundaries. However, the final number of microphones is not known a priori, since it depends on the overlap between the initial circular arrangement and the polygonal mask. Therefore, the number of microphones or the radius of the initial circular array may have to be adjusted iteratively until the masked arrangement contains approximately the desired number of sensors. In addition, masking can remove microphones unevenly near the boundary, which may locally affect the density and coarray properties of the resulting arrangement.

A third strategy is to synthesize the microphone positions directly inside the target domain by means of a weighted centroidal Voronoi tessellation (CVT) [14]. In contrast to the transformation and masking approaches, this method does not start from an existing circular phyllotactic arrangement. Consequently, some of the preferable properties of the original spiral construction, such as its deterministic angular progression and phyllotactic ordering, are not explicitly preserved. However, the method is well suited for arbitrary geometries and allows spatial density variations to be incorporated in a natural way.

Let Ω denote the desired array domain and let $\{\mathbf{x}_i\}_{i=1}^{N}$ be a set of generator points corresponding to the microphone positions. These points define a Voronoi tessellation of Ω, where each Voronoi cell

$$V_i = \left\{ \mathbf{x} \in \Omega \;\middle|\; \|\mathbf{x}-\mathbf{x}_i\| \leq \|\mathbf{x}-\mathbf{x}_j\|, \quad j = 1,\ldots,N \right\} \tag{18}$$

contains all positions in the domain that are closer to $\mathbf{x}_i$ than to any other generator. In a weighted CVT, a non-negative density function $w(\mathbf{x})$ such as the Hansen weight is prescribed over the domain. Each generator is then moved to the weighted centroid of its Voronoi cell,

$$\mathbf{x}_i = \frac{\int_{V_i} \mathbf{x}\, w(\mathbf{x})\, d\mathbf{x}}{\int_{V_i} w(\mathbf{x})\, d\mathbf{x}}. \tag{19}$$

Starting from an initial set of points, this update is applied iteratively: the Voronoi cells are computed, their weighted centroids are evaluated, and the generator points are replaced by these centroids. The iteration is repeated until the movement of the points becomes sufficiently small.

The density function $w(\mathbf{x})$ controls the local spacing of the microphones. Regions with larger weight attract more generator points and therefore lead to a locally higher microphone density, while regions with smaller weight are sampled more sparsely. This makes weighted CVT particularly useful when a desired aperture weighting should be realized geometrically in a non-circular domain. At the same time, because the resulting arrangement is determined by the chosen density function, the boundary shape, and the initialization, the final layout should be regarded as an optimized spatial distribution rather than a transformed phyllotactic spiral.

In the numerical implementation, the weighted centroids are evaluated by quasi-Monte Carlo quadrature. For this purpose, a Sobol sequence [15] is generated over the bounding box of the target domain, and only points located inside Ω are retained. To obtain a sufficiently dense numerical representation of the domain, the number of quadrature points is chosen to be at least $500N$, where N is the number of microphones. The weighted centroid of the i-th Voronoi cell is then approximated by

$$\mathbf{x}_i \approx \frac{\sum_{\mathbf{q}_k \in V_i} \mathbf{q}_k\, w(\mathbf{q}_k)}{\sum_{\mathbf{q}_k \in V_i} w(\mathbf{q}_k)}, \tag{20}$$

where $\mathbf{q}_k$ are the retained Sobol quadrature points assigned to the cell V_i. The use of a low-discrepancy Sobol sequence provides a more uniform coverage of the integration domain than purely random sampling, which reduces numerical noise in the centroid estimates and improves the stability of the CVT iteration.

3 Evaluation Methodology

The different microphone arrangements are evaluated by means of their point spread function (PSF). For this purpose, a single unit-strength monopole source is assumed at a reference position on the scan grid, and the resulting beamforming map is computed over the complete evaluation plane. The PSF is calculated using the steering vector formulation IV [16], which is commonly used for three-dimensional source mapping and provides a consistent basis for comparing array geometries. The PSF is normalized with respect to its maximum value, such that all array arrangements can be compared independently of their absolute gain.

Three scalar quantities are extracted from the normalized PSF. The first measure is the half-power main-lobe width, which characterizes the spatial extent of the main lobe and therefore the resolution of the array. It is defined as the width of the main lobe at the level

$$B(\mathbf{x}) = \frac{1}{2} B_{\max}, \tag{21}$$

or equivalently at $-3\,\mathrm{dB}$ when the PSF is expressed in decibels. Here, $B(\mathbf{x})$ denotes the normalized PSF value at scan position $\mathbf{x}$ and $B_{\max}$ is the maximum value of the PSF. In practice, the half-power width is determined from the connected region around the PSF maximum for which

$$B(\mathbf{x}) \geq \frac{1}{2} B_{\max}. \tag{22}$$

A smaller half-power main-lobe width indicates a higher spatial resolution.

The second measure is the maximum side-lobe level. This quantity describes the highest PSF value outside the main-lobe region and is therefore an indicator of the strongest ghost source that may be produced by the array. After excluding the main-lobe region Ω_{ML}, the maximum side-lobe level is computed as

$$L_{\mathrm{SL,max}} = 10 \log_{10} \left(\frac{\max_{\mathbf{x} \notin \Omega_{\mathrm{ML}}} B(\mathbf{x})}{B_{\max}} \right). \tag{23}$$

Since the PSF is normalized to its maximum, this value is non-positive when expressed in decibels. Lower values indicate better suppression of the strongest side lobe.

The third measure is the integrated side-lobe level [17], which quantifies the total energy contained in the side-lobe region rather than only the largest side-lobe peak. It is computed by integrating the normalized PSF outside the main-lobe region,

$$L_{\mathrm{SL,int}} = 10 \log_{10} \left(\frac{\int_{\Omega \setminus \Omega_{\mathrm{ML}}} B(\mathbf{x})\, d\mathbf{x}}{\int_{\Omega_{\mathrm{ML}}} B(\mathbf{x})\, d\mathbf{x}} \right), \tag{24}$$

where Ω denotes the complete evaluation domain. For a discretized scan grid, the integrals are replaced by sums over the respective grid points,

$$L_{\mathrm{SL,int}} = 10 \log_{10} \left(\frac{\sum_{\mathbf{x}_j \notin \Omega_{\mathrm{ML}}} B(\mathbf{x}_j)}{\sum_{\mathbf{x}_j \in \Omega_{\mathrm{ML}}} B(\mathbf{x}_j)} \right). \tag{25}$$

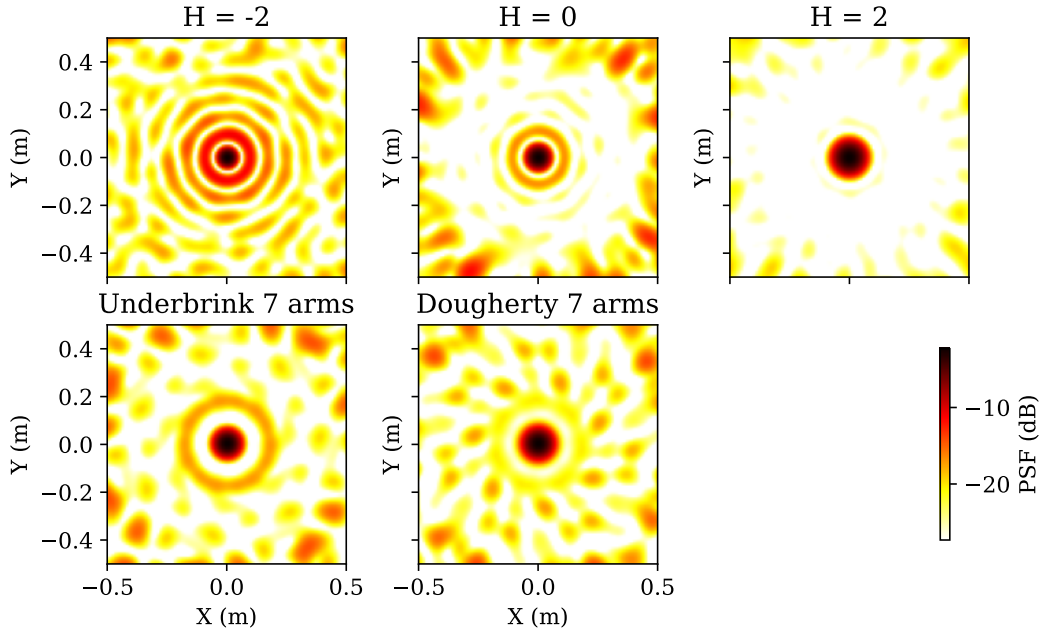

Figure 4: Example PSFs for different spiral geometries with aperture radius $r_{\max} = 1.0$, $N = 64$ microphones, He $= 20$*, and mapping distance $d = 1.0$. The examples illustrate differences in main-lobe extent, maximum side-lobe level, and overall side-lobe distribution.*

While the maximum side-lobe level captures the most critical isolated artifact, the integrated side-lobe level reflects the overall distribution of side-lobe energy over the scan region. The three measures therefore characterize complementary aspects of array performance: spatial resolution, strongest ambiguity, and total side-lobe contamination.

The main-lobe region is defined as the connected region around the PSF maximum whose level is less than 3 dB below the maximum value. With the normalized PSF denoted by $B(\mathbf{x})$ and $B_{\max} = \max_{\mathbf{x}} B(\mathbf{x})$, this region is given by

$$\Omega_{\mathrm{ML}} = \left\{ \mathbf{x} \;\middle|\; B(\mathbf{x}) \geq \frac{1}{2} B_{\max} \right\}_{\text{connected to } \mathbf{x}_{\max}}. \tag{26}$$

The half-power main-lobe width is then expressed as the apparent radius of this region. For a two-dimensional scan plane, this radius is computed from the area of the main-lobe region according to

$$r_{\mathrm{ML}} = \sqrt{\frac{|\Omega_{\mathrm{ML}}|}{\pi}}, \tag{27}$$

where $|\Omega_{\mathrm{ML}}|$ denotes the area enclosed by the half-power contour. For a discretized scan grid with uniform cell area ΔA, this becomes

$$r_{\mathrm{ML}} = \sqrt{\frac{N_{\mathrm{ML}} \Delta A}{\pi}}, \tag{28}$$

where N_{ML} is the number of grid cells belonging to the connected half-power region. This definition provides a scalar measure of the effective main-lobe size that remains applicable even when the main lobe is not perfectly circular.

The apparent radius of the main lobe depends on both the frequency and the distance d of the mapping plane from the array. To allow for a meaningful comparison of different array geometries, the main-lobe width is normalized by estimating the angle subtended by the main lobe as

$$\alpha_{\mathrm{ML}} = 2\arctan\left(\frac{r_{\mathrm{ML}}}{d}\right), \tag{29}$$

and the frequency is given by the Helmholtz number

$$\mathrm{He} = \frac{f r_{\max}}{c}, \tag{30}$$

where f is the frequency, $r_{\max}$ is the maximum array radius, and c is the speed of sound.

4 Results

4.1 Beamforming Performance of Spiral Arrays

The beamforming performance of the considered spiral arrangements is first evaluated in terms of the trade-off between main-lobe width and side-lobe suppression. Figure 5 shows the relationship between the apparent main-lobe angle and the maximum side-lobe level for Vogel spirals with different radial weighting parameters H, together with Dougherty and Underbrink spirals for different numbers of spiral arms.

The Vogel arrangements form a clear Pareto frontier, confirming earlier observations from the literature that phyllotaxis-based microphone arrays provide highly favorable beamforming characteristics. As the weighting parameter H is varied, the resulting arrays continuously trade spatial resolution against side-lobe suppression. Arrangements with smaller main-lobe angles generally exhibit increased maximum side-lobe levels, whereas stronger radial weighting reduces the side-lobe level at the expense of a broader main lobe. No arrangement simultaneously minimizes both quantities, which is consistent with the multi-objective nature of the array synthesis problem discussed previously.

The Dougherty and Underbrink spirals approach the Pareto frontier only when several spiral arms are used. Single-arm variants exhibit noticeably inferior beamforming performance, which can be attributed to their less homogeneous aperture coverage and more anisotropic coarray structure. Increasing the number of arms improves the angular distribution of microphone positions and reduces the discrepancy relative to the Vogel arrangements. Nevertheless, the generalized phyllotaxis arrays consistently provide the most favorable compromise between main-lobe width and maximum side-lobe level over the investigated parameter range.

These observations are in good agreement with previously published results on sunflower-type arrays and confirm that the present implementation reproduces the known Pareto-optimal behavior of weighted Vogel arrangements. Figure 6 shows the corresponding results for the integrated side-lobe level. The overall behavior is qualitatively very similar to that observed for the maximum side-lobe level. In particular, the Vogel arrangements again form a Pareto-like frontier, while the multi-arm Underbrink and Dougherty spirals approach this frontier only

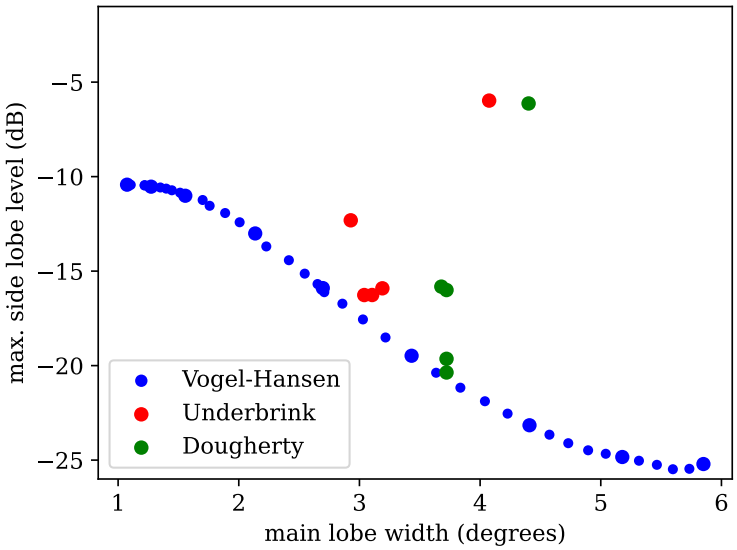

Figure 5: Pareto-like frontier of beamforming performance given by main lobe width and maximum side-lobe level for different radial weightings of the Vogel spiral and $\mathrm{He} = 20$*. The points correspond to different values of the weighting parameter* H*. Highlighted markers correspond to integer weights* $H = -4,-3,\ldots,3,4$*. Underbrink and Dougherty spirals with different number of arms* ($M = 1,3,5,7,9$) *are included for comparison.*

for larger numbers of arms. Since the integrated side-lobe level does not reveal substantially different trends from the maximum side-lobe level, the following discussion focuses primarily on the latter quantity.

The preceding results demonstrate the favorable beamforming characteristics of weighted Vogel spirals for disk-like apertures. In the following, these arrangements are adapted to non-circular domains using the geometric transformation, masking, and weighted CVT approaches introduced previously. In all cases, a radial weighting parameter of $H = 1$ is used as a representative compromise between main-lobe width and side-lobe suppression.

Three representative aperture shapes are considered, namely a square, a rectangle, and a cross-shaped domain, shown in Figure 7. The largest edge length is normalized to 2.0 in all cases in order to allow a consistent comparison of the resulting beamforming characteristics.

Figures 8–10 show the resulting microphone arrangements together with the corresponding PSFs for the three geometric adaptation strategies. For the square aperture, all three methods produce comparatively similar array layouts and PSF characteristics. In particular, the mapped and masked arrangements preserve much of the isotropic structure of the original phyllotactic distribution, while the weighted CVT produces a slightly more homogeneous spatial distribution. The resulting beamforming performance differs only moderately between the three approaches.

For the rectangular and cross-shaped apertures, the differences between the adaptation strategies become more pronounced. The mapping approach increasingly distorts the original phyllotactic structure as the target geometry deviates from a circular domain. This leads to locally

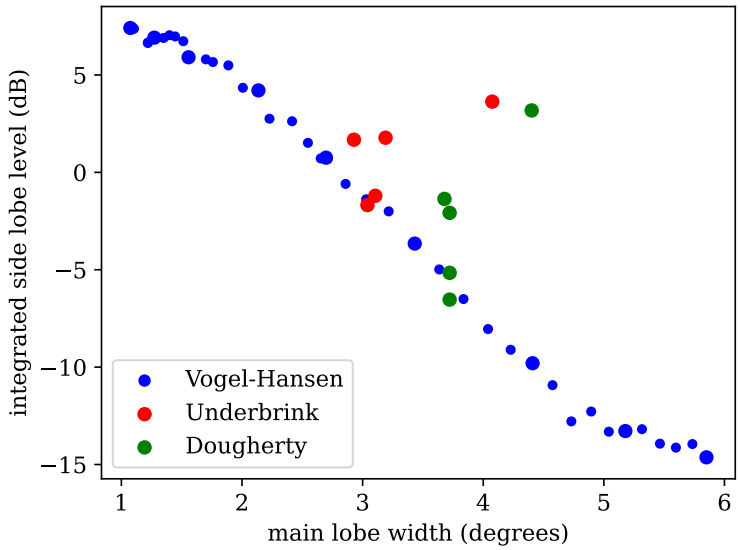

Figure 6: Same as Figure 5, but showing the integrated side-lobe level for the same set of spiral geometries.

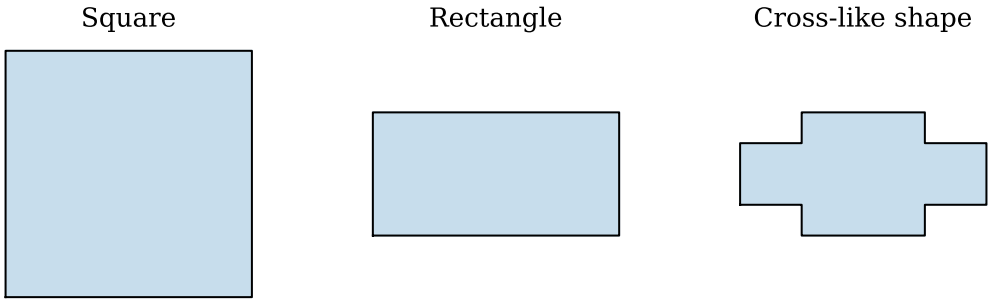

Figure 7: The three array shapes considered in the present study. The largest edge length is always 2.0.

stretched or compressed regions in the microphone distribution and produces more pronounced directional artifacts in the PSF. The effect is particularly visible for the cross-shaped aperture, where the mapped arrangement exhibits noticeable anisotropy and elevated side-lobe structures.

The masking approach generally preserves the local structure of the original Vogel arrangement more successfully, since the remaining microphones retain the underlying phyllotactic ordering. However, the removal of microphones near the boundary introduces local density variations and irregular truncation effects, which become increasingly significant for strongly non-convex geometries.

Among the investigated approaches, the weighted CVT method consistently yields the most homogeneous microphone distributions and the most favorable PSF characteristics. Since the CVT directly optimizes the spatial distribution inside the target domain, it naturally adapts to arbitrary boundaries without introducing the geometric distortions associated with explicit coordinate mappings. At the same time, the weighting function allows the radial density distribution

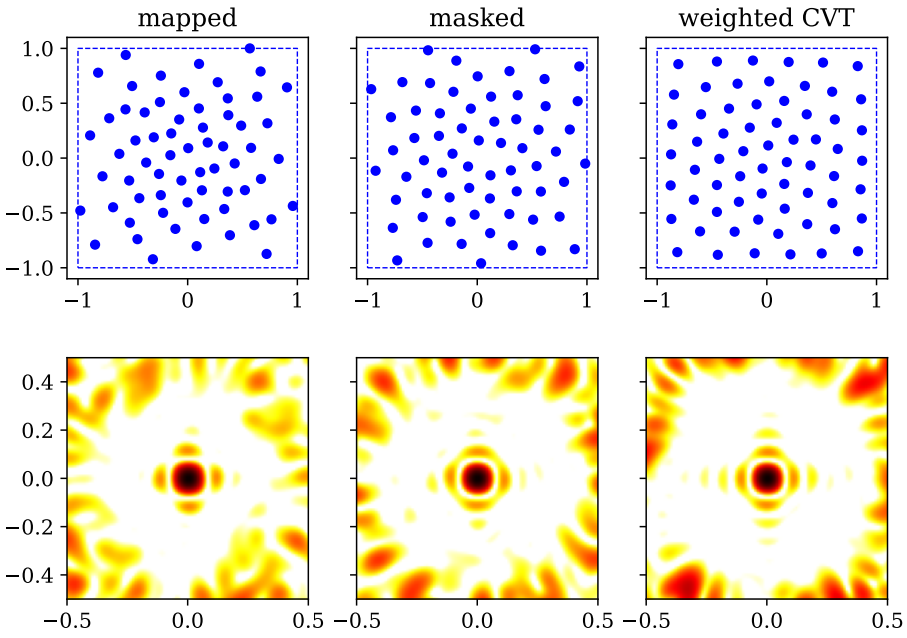

Figure 8: Square microphone arrangements obtained by geometric mapping, masking, and weighted centroidal Voronoi tessellation together with the corresponding normalized PSFs.

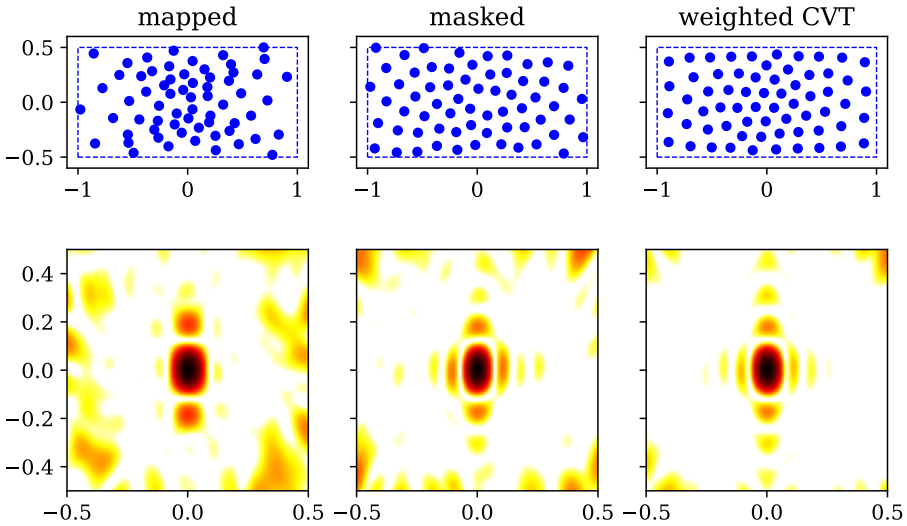

Figure 9: Rectangular microphone arrangements obtained by geometric mapping, masking, and weighted centroidal Voronoi tessellation together with the corresponding normalized PSFs.

of the original phyllotactic arrangement to be incorporated in a straightforward manner.

The quantitative comparison shown in Figure 11 confirms these observations. For the square aperture, all three adaptation strategies remain relatively close in terms of the trade-off between

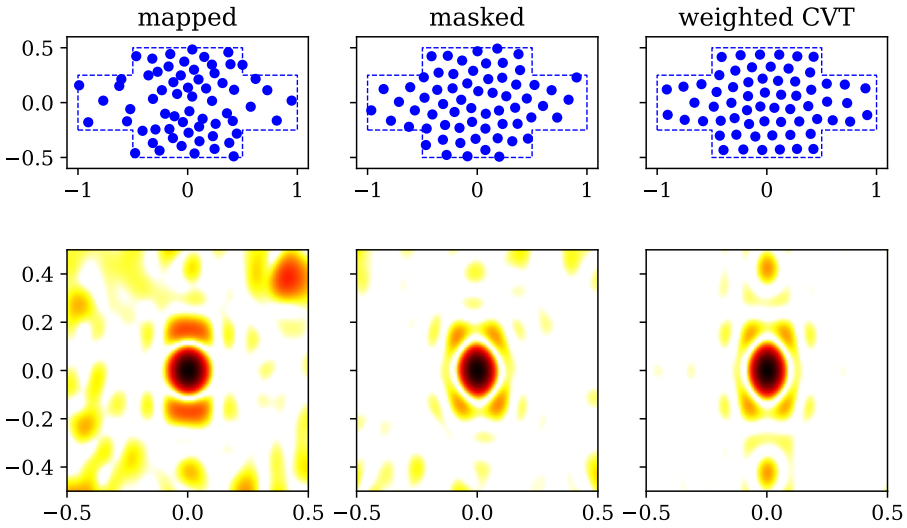

Figure 10: Cross-shaped microphone arrangements obtained by geometric mapping, masking, and weighted centroidal Voronoi tessellation together with the corresponding normalized PSFs.

main-lobe width and side-lobe suppression. For increasingly non-circular geometries, however, the mapped arrangements move away from the Pareto-like region established by the disk-like Vogel spirals. The masking approach generally performs better, while the weighted CVT arrangements consistently provide the most favorable compromise between spatial resolution and side-lobe suppression across all investigated aperture shapes.

These results indicate that the favorable beamforming properties of phyllotactic arrays can largely be preserved under geometric adaptation, provided that the adaptation strategy maintains a sufficiently homogeneous and isotropic spatial distribution. In this respect, weighted CVT synthesis appears particularly attractive because it combines geometric flexibility with direct control over the spatial density distribution.

5 Discussion

Among the investigated adaptation strategies, geometric mapping provides the most direct transformation of the original spiral arrangement. However, its performance deteriorates for strongly non-circular or non-convex domains because the mapping introduces local stretching and compression effects. In contrast, masking and weighted centroidal Voronoi tessellation (CVT) preserve a more homogeneous spatial distribution and therefore yield more robust beamforming characteristics for complex geometries.

An important practical advantage of masking and weighted CVT approaches is their applicability to domains containing holes or excluded regions, as frequently encountered in wind-tunnel installations, mounting structures, or measurement windows. In such cases, a direct geometric mapping from a circular aperture becomes difficult or impossible to define consistently. Masking naturally accommodates excluded regions by removing microphones located inside forbidden areas, while weighted CVT can incorporate such constraints directly into the

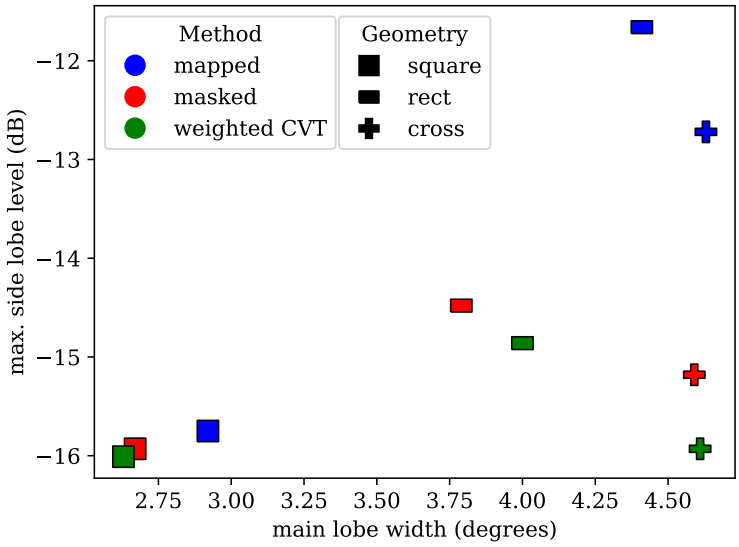

Figure 11: Results comparison for square, rectangular, and cross-shaped array geometries and different geometric adaptation strategies.

tessellation domain.

For disconnected or strongly fragmented domains, however, masking currently remains the most straightforward approach because it preserves the local structure of the underlying phyllotactic arrangement independently of the global domain connectivity. The present weighted CVT implementation assumes a connected domain and may therefore require modifications for non-continuous geometries. Nevertheless, there is no fundamental limitation preventing an extension of the CVT approach to disconnected regions, for example by introducing multiple coupled tessellation domains or connectivity-aware initialization strategies.

The present investigation focuses primarily on beamforming-based performance measures derived from the point spread function. Consequently, the reported results do not directly establish the behavior of the investigated geometries for other reconstruction techniques such as deconvolution or inverse methods. Nevertheless, many acoustic imaging algorithms ultimately rely on the spatial information encoded in the pairwise phase differences between microphones, which are determined by the coarray structure of the arrangement. Since the investigated phyllotactic and CVT-based geometries provide broad and comparatively homogeneous distributions of pairwise separations, it is reasonable to expect that their favorable spatial sampling properties will also benefit more advanced reconstruction algorithms.

At the same time, deconvolution and inverse approaches partially compensate for the PSF limitations of conventional beamforming through regularization or iterative reconstruction procedures. Their sensitivity to particular side-lobe structures may therefore differ substantially from that observed for beamforming alone [18]. In this respect, the beamforming-based evaluation used in the present work should primarily be interpreted as a baseline characterization of the underlying spatial sampling properties rather than as a complete predictor of reconstruction quality for all imaging algorithms.

Several limitations of the present study should be noted. First, only planar two-dimensional arrangements were considered, whereas practical applications may also require curved or fully

three-dimensional arrays. Second, the evaluation was restricted to idealized free-field conditions and did not include measurement noise, calibration errors, flow effects, or scattering structures. Third, the investigated performance measures characterize only the static PSF properties of the arrays and do not address computational complexity, robustness against sensor failure, or broadband optimization criteria. These aspects provide promising directions for future work.

Future investigations could therefore extend the proposed geometric adaptation strategies to three-dimensional apertures, incorporate application-specific weighting functions, and evaluate the resulting arrangements using deconvolution and inverse reconstruction techniques under realistic experimental conditions.

6 Conclusion

The present study investigated the influence of microphone-array geometry on acoustic imaging performance and compared several strategies for generating planar array arrangements. Starting from phyllotaxis-based spiral arrays, different radial weighting schemes and geometric adaptation methods were analyzed with respect to their point spread function characteristics. The results confirm the favorable beamforming properties of weighted Vogel spirals and reproduce the Pareto-like trade-off between main-lobe width and side-lobe suppression reported in earlier work.

Different strategies for adapting disk-like arrangements to non-circular domains were evaluated, including geometric mapping, masking, and weighted centroidal Voronoi tessellation. While all approaches produced comparable results for mildly non-circular geometries, weighted CVT arrangements consistently yielded the most robust overall performance for more complex domains. At the same time, masking proved particularly attractive for geometries containing holes or disconnected regions.

Overall, the results demonstrate that favorable spatial sampling properties can be preserved beyond circular apertures, provided that the geometric adaptation maintains a sufficiently homogeneous and isotropic distribution of pairwise microphone separations. The presented methods therefore provide a flexible framework for constructing microphone arrays tailored to practical measurement constraints while retaining advantageous beamforming characteristics. Future work should investigate the behavior of these arrangements for deconvolution and inverse reconstruction methods as well as under realistic experimental conditions.

Acknowledgment

References

[1] R. P. Dougherty, “Spiral-shaped arrays for broadband imaging,” 1998, pat. US 5,838,284.

[2] J. R. Underbrink, “Aeroacoustic phased array testing in low speed wind tunnels,” in *Aeroacoustic Measurements*, T. J. Mueller, Ed. Springer, 2002, pp. 98–217.

[3] E. Sarradj, “A generic approach to synthesize optimal array microphone arrangements,” in *Proceedings of the 6th Berlin Beamforming Conference*, 2016.

[4] C. Puhle, S. Barré, and S. Hollands, "On the sunflower spiral: Acoustical holography results," in *Proceedings Internoise*, 2016.

[5] A. Malgoezar, M. Snellen, P. Sijtsma, and D. Simons, "Improving beamforming by optimization of acoustic array microphone positions," in *Proceedings of the 6th Berlin Beamforming Conference*, 2016.

[6] E. Arcondoulis and Y. Liu, "An iterative microphone removal method for acoustic beamforming array design," *Journal of Sound and Vibration*, vol. 442, pp. 552–571, 2019.

[7] S. M. Khatami and M. Y. A. Jamalabadi, "Optimal design of microphone array in a planar circular configuration by genetic algorithm enhanced beamforming," *Journal of Thermal Analysis and Calorimetry*, vol. 143, pp. 3825–3837, 2020.

[8] Y. Wang, Z. Deng, J. Zhao, V. F. Kopiev, D. Gao, and W.-L. Chen, "Progress in beamforming acoustic imaging based on phased microphone arrays: Algorithms and applications," *Measurement*, vol. 242, p. 116100, 2025.

[9] J. Xiong, X. Zha, X. Pei, and W. Zhou, "Topology optimization design method for acoustic imaging array of power equipment," *Sensors*, vol. 24, no. 7, 2024.

[10] Y. Zhang, Z. Li, and K. F. C. Yiu, "Optimal microphone array placement design using the bayesian optimization method," *Sensors*, vol. 24, no. 8, 2024.

[11] H. Vogel, "A better way to construct the sunflower head," *Mathematical Biosciences*, vol. 44, no. 3–4, pp. 179–189, 1979.

[12] R. C. Hansen, *Phased array antennas*. John Wiley & Sons, 2001.

[13] T. A. Driscoll and L. N. Trefethen, *Schwarz–Christoffel Mapping*, ser. Cambridge Monographs on Applied and Computational Mathematics. Cambridge University Press, 2002, vol. 8.

[14] Q. Du, V. Faber, and M. Gunzburger, "Centroidal voronoi tessellations: Applications and algorithms," *SIAM Review*, vol. 41, no. 4, pp. 637–676, 1999.

[15] C. Lemieux, *Monte Carlo and Quasi-Monte Carlo Sampling*, ser. Springer Series in Statistics. Springer, 2009.

[16] E. Sarradj, "Three-dimensional acoustic source mapping with different beamforming steering vector formulations," *Advances in Acoustics and Vibration*, vol. 2012, p. 292695, 2012.

[17] H. L. V. Trees, *Optimum Array Processing*, ser. Detection, Estimation, and Modulation Theory, Part IV. Wiley, 2002.

[18] G. Herold and E. Sarradj, "Performance analysis of microphone array methods," *Journal of Sound and Vibration*, vol. 401, pp. 152–168, 2017.